HHS Public Access

Author manuscript

ACS Appl Mater Interfaces. Author manuscript; available in PMC 2023 May 27.

Published in final edited form as:

ACS Appl Mater Interfaces. 2022 March 23; 14(11): 13631–13637. doi:10.1021/acsami.1c25215.

Ultrabright Pdots with a large absorbance cross section and high quantum yield

Jicheng Zhang,

Jiangbo Yu,

Yifei Jiang,

Daniel T. Chiu*

Departments of Chemistry and Bioengineering, University of Washington, Seattle, WA 98195

Abstract

Semiconducting polymer dots (Pdots) are increasingly used in biomedical applications due to their extreme single-particle brightness, which results from their large absorption cross section (σ). However, the quantum yield (Φ) of Pdots is typically below 40% due to aggregation-induced self-quenching. One approach to reduce self-quenching is to use FRET between donor (D) and acceptor (A) groups within a Pdot; however, Φ values of FRET-based Pdots remain low. Here we demonstrate an approach to achieve ultra-bright FRET-based Pdots with simultaneously high σ and Φ. The importance of self-quenching was revealed in a non-FRET Pdot: adding 30 mol% of a non-absorbing polyfluorene to a poly(9,9-dioctylfluorene) (PFO) Pdot increased Φ from 13.4% to 71.2%, yielding an ultra-bright blue-emitting Pdot. We optimized the brightness of FRET-based Pdots by exploring different D/A combinations and ratios with PFO and poly[(9,9-dioctylfluorenyl-2,7-diyl)-co-(1,4-phenylene) (PFP) as donor polymers and poly[(9,9-dioctyl-2,7-divinylenefluorenylene)-alt-co-(1,4-phenylene)] (PFPV) and poly[(9,9-dioctylfluorenyl-2,7-diyl)-alt-co-(1,4-benzo-{2,1',3}-thiadiazole)] (PFBT) as acceptor polymers, and with a fixed concentration of poly(styrene-co-maleic anhydride) as surfactant polymer. Ultra-bright blue-emitting Pdots possessing high Φ (73.1%) and σ ($\sigma_R=\sigma_{abs}/\sigma_{all}$, 97.5%) were achieved by using PFP/PFPV Pdots at a low acceptor content (A/[D+A], 2.5 mol%). PFP/PFPV Pdots were 1.8 times as bright as PFO/PFPV Pdots due to greater coverage of acceptor absorbance by donor emission—a factor often overlooked in D/A pair selection. Ultra-bright green-emitting PFO Pdots (Φ=76.0%, σ_R=92.5%) were obtained by selecting an acceptor (PFBT) with greater spectral overlap with PFO. Ultra-bright red-emitting Pdots (Φ=64.2%, σ_R=91.0%) were achieved by blending PFO, PFBT, and PFTBT to create a cascade FRET Pdot at a D:A_1:A_2 molar ratio of 61:5:1. These blue, green, and red Pdots are among the brightest Pdots reported. This approach of

***Corresponding Author:** D. T. Chiu - Departments of Chemistry and Bioengineering, University of Washington, Seattle, WA 98195, United States; chiu@uw.edu.

J. Zhang – Department of Chemistry, University of Washington, Seattle, WA 98133, United States

J. Yu - Department of Chemistry, University of Washington, Seattle, WA 98133, United States

Y. Jiang - Department of Chemistry, University of Washington, Seattle, WA 98133, United States

* Supporting Information

The Supporting Information is available free of charge on the ACS Publications website.

Polymer structure and synthesis route; absorption and emission of PFO, PFP, PFO/PF, PFO/PFBT, and PFO/PFBT/PFTBT Pdots with different acceptor contents; Jablonski diagram illustrating the mechanism of cascade FRET in PFO/PFBT/PFTBT Pdots.

D.T.Chiu and J.Yu have financial interest in Lamprogen Inc., which has licensed the technology from the University of Washington.

using a small, optimized amount of FRET acceptor polymer with a large donor-acceptor spectral overlap can be generalized to produce ultra-bright Pdots with emissions that span the visible spectrum.

Graphical Abstract

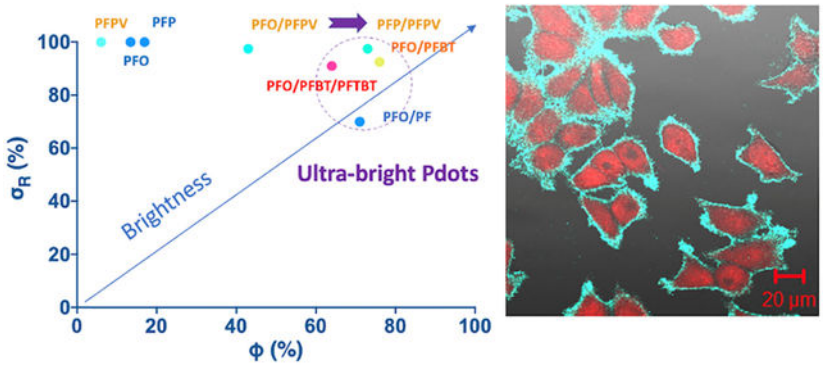

Keywords

semiconducting polymer dots (Pdots); ultra-bright; FRET; quantum yield; absorption cross section

1. INTRODUCTION

Semiconducting polymer dots (Pdots) are over an order of magnitude brighter than small molecule organic dyes, fluorescent proteins, and other fluorescent nanoparticles such as quantum dots (Qdots), which results from their large absorption cross section (σ),[1–3] and have tunable absorption and emission, and good photostability and biocompatibility.[4] As a result, Pdots have been increasingly used as fluorescent probes in biosensors and bioimaging including super-resolution imaging.[5–16] Pdots have been developed with emissions that span the visible spectrum,[17] but ultra-bright Pdots with both large absorption cross section (σ) and high quantum yield (Φ) have been elusive. Strategies to increase Pdot brightness have focused on increasing Φ by reducing aggregation-induced self-quenching by using excess surfactant polymer,[18] twisted molecular structures,[19] bulky side chains,[3] or reduced concentration of fluorescent units.[20] However, these approaches have resulted in lower σ. An alternate strategy to increase Pdot brightness is to use FRET between a large number of excited donor (D) groups and a small number of acceptor (A) groups to reduce self-quenching while retaining high σ.[21–23] However, the brightness of FRET-based Pdots has been limited by low Φ values.[5]/16/2023 10:28:00 AM

In FRET, dipole–dipole coupling results in non-radioactive energy transfer from the excited state of a donor to a nearby acceptor.[24–26] FRET efficiency is highly dependent on the distance R between donor and acceptor, falling off as $1/R^6$. FRET efficiency also depends on donor-acceptor spectral overlap, which includes not only the coverage of donor emission by acceptor absorbance but also the coverage of acceptor absorbance by donor emission. In Pdots, FRET can occur both within and between polymer chains (the maximum effective distance of FRET is ~10 nm;[24] Pdots are 5–30 nm in diameter); therefore, blending

of donor and acceptor polymers can be used to fabricate Pdots with efficient interchain energy transfer. This blending approach facilitates screening different FRET donor-acceptor combinations and ratios to optimize Pdot brightness while avoiding multi-step synthesis.

Here we optimized Pdot brightness by exploring different pairs of FRET donor- and acceptor-containing polymers and blended Pdot compositions to create D/A and D/A_1/A_2 (cascade FRET) Pdots. We first explore the importance of reducing aggregation-induced self-quenching in a non-FRET Pdot by incorporating different amounts of a non-absorbing polymer to optimize Pdot brightness. The blending method for synthesizing FRET-based Pdots facilitates the screening of different donor-acceptor pairs and ratios and avoids complicated Pdot synthesis. The strategy presented here can be generalized to produce ultra-bright Pdots with emissions that span the visible spectrum.

2. EXPERIMENTAL SECTION

2.1. Materials.

Poly(9,9-dioctylfluorene) (PFO, M_w=2.5×10^4 Da), poly[(9,9-dioctylfluorenyl-2,7-diyl)-co-(1,4-phenylene)] (PFP, M_w=2.5×10^4 Da), poly[(9,9-dioctylfluorenyl-2,7-diyl)-alt-co-(1,4-benzo-{2,1’,3}-thiadiazole)] (PFBT, M_w=1.5×10^4 Da), and poly[(9,9-dioctyl-2,7-divinylenefluorenylene)-alt-co-(1,4-phenylene)] (PFPV, M_w=2.0×10^4 Da) were purchased from America Dye Source, Inc. (Quebec, Canada). Poly(styrene-co-maleic anhydride) (PSMA, M_n=1.9×10^3 Da) and other chemicals and solvents were purchased from Sigma-Aldrich (St. Louis, MO, USA).

2.2. Instruments.

Transmission electron microscopy (TEM) of Pdots was performed with a Tecnai F20 TEM (FEI; Hillsboro, OR, USA). Hydrodynamic sizes of Pdots were characterized by dynamic light scattering (DLS) with a Zetasizer Nano S (Malvern Panalytical; Malvern, UK). UV-Vis absorption spectra were recorded with a DU 720 scanning spectrophotometer (Beckman Coulter, Inc.; Pasadena, CA, USA). Fluorescence spectra of Pdots in solution were collected with a Fluorolog-3 fluorometer (HORIBA Jobin Yvon; Edison, NJ, USA). Fluorescence quantum yields of Pdots in solution were measured with a Hamamatsu photonic multichannel analyzer C10027 (Hamamatsu; Hamamatsu City, Japan) with a CCD integrating sphere. Calibration of fluorescence intensity measurements was performed using Coumarin-102 dye (Sigma-Aldrich).

2.3. Polymer synthesis.

Poly[(2,3-dimethyl-1,4-phenylene)-co-(1,4-phenylene)] (PF) was synthesized using the monomers 1,4-benzenediboronic acid bis(pinacol) ester (0.2 mmol) and 1,4-dibromo-2,3-dimethylbenzene (0.2 mmol). A mixture of the monomers, Aliquat 336 (1 drop), $Pd(PPh_3)_4$ (5 mg; 0.005 mmol), 2 M aqueous Na_2CO_3 (3 mL), and toluene (6 mL) was degassed under nitrogen. The mixture was stirred at 90 °C for 6 h then the polymer was end-capped with 0.1 M phenylboronic acid (1 mL) and bromobenzene (1 mL). After cooling, the reaction mixture was poured into 100 mL of methanol and filtered. The precipitate was collected and dissolved in 50 mL of dichloromethane, washed three times with 50 mL of water,

dried with anhydrous Na_2SO_4 then redissolved in 5 mL of dichloromethane. After filtration through a 0.2-μm pore size PVDF syringe filter and evaporating the solvent, the residue was precipitated by stirring in 100 mL of methanol. A white product was obtained after drying in vacuum, with a yield of 32% (M_n=7.2×10^3 Da, PDI=2.2).

Poly((9,9-dioctylfluorene)-2,7-diyl-alt-[4,7-bis(3-hexylthien-5-yl)-2,1,3-benzothiadiazole]-2',2"-diyl) (PFTBT) was synthesized as above except using the monomers 9,9-dioctylfluorene-2,7-diboronic acid pinacol ester (0.2 mmol), 9,9-dioctyl-2,7-dibromofluorene (0.18 mmol), and 4,7-bis(5-bromothiophen-2-yl)benzo[c][1,2,5]thiadiazole (0.18 mmol). A red product was obtained after drying in vacuum, with a yield of 86% (M_n=3.7×10^4 Da, PDI=2.3).

2.4. Pdot preparation.

Pdots were prepared by co-nanoprecipitation as described previously.[2] Polymers including PSMA were dissolved individually in anhydrous THF at 1 mg/mL, then were mixed at different D:A ratios to obtain a total semiconducting polymer concentration of 0.2 mg/mL and a PSMA concentration of 0.04 mg/mL. 5 mL of the mixed polymers in THF was injected into 10 mL of MilliQ water under sonication. THF was removed by nitrogen stripping and the solution was concentrated to 5 mL by continuous nitrogen stripping on a 90 °C hotplate followed by filtration through a 0.22-μm pore size cellulose nitrate syringe filter.

2.5. Bioconjugation.

Pdots were conjugated with streptavidin in an EDC-catalyzed reaction between Pdot carboxyl groups and streptavidin amine groups. 80 μL of polyethylene glycol (PEG, M_W 3350 Da, 5% w/v) and 80 μL of 1 M HEPES pH 7.4 buffer were added to 4 mL of COOH-functionalized Pdots (50 μg/mL in MilliQ water), resulting a final HEPES concentration of 20 mM. 240 μL of 1 mg/mL streptavidin solution (Invitrogen; Eugene, OR, USA) was added and the mixture was vortexed. Freshly prepared EDC solution (80 μL, 5 mg/mL in MilliQ water) was added, and the solution was mixed on a rotary shaker for 3 h at room temperature. BSA (2% w/v, 20 μL) and Triton-X 100 (0.25% w/v, 20 μL) were added and the mixture was stirred for 30 min then mixed for an additional 1 h on a rotary shaker. Pdot bioconjugates were separated from unbound biomolecules by gel filtration with Sephacryl HR-300 gel media.

2.6. Cell culture.

MCF-7 breast cancer cells and Jurkat T lymphoblastoid cells were purchased from American Type Culture Collection (ATCC; Manassas, VA, USA). MCF-7 cells were cultured at 37 °C, 5% CO_2 in Eagle's minimum essential medium with 10% w/v fetal bovine serum (FBS; Hyclone Laboratories, Inc.; Logan, UT, USA), 50 U/mL penicillin, and 50 μg/mL streptomycin. The cells were cultured to confluence and were harvested by rinsing with culture media then incubating with 5 mL of 0.25% w/v trypsin and 0.53 mM EDTA at 37 °C for 5–15 min until detachment. The detached cells were rinsed, centrifuged, and resuspended in PBS buffer. Jurkat T lymphoblastoid cells were cultured in advanced

RPMI 1640 medium (Gibco / Thermo Fisher; Waltham, MA, USA) with 10% FBS, 10 mM HEPES, 100 U/mL penicillin, and 100 μg/mL streptomycin at 37 °C and 5% CO_2.

For Pdot toxicity studies, BS-C-1 cells (African green monkey kidney, ATCC #CCL-26) were seeded on 8-well chamber slides and incubated with PFP/PFPV blue-emitting Pdots, PFO/PFBT-BT green-emitting Pdots, and PFO/PFBT/PFTBT-TBT red-emitting Pdots. After incubation of BS-C-1 cells with 50 ppm Pdots for 24 hr, the cells were studied under the microscope. From the fluorescence images of these cells, it can be seen these three types of Pdots were endocytosed by the cells. Furthermore, the cells appear healthy and continued to divide, consistent with our prior reports on the non-toxic nature of Pdots on cells (Figure. S5).[2, 27]

2.7. Cellular imaging.

The fluorescence images of MCF-7 cells were acquired using a confocal microscope (Zeiss LSM 510). The blue channel was excited by a 405 nm diode laser. An EC Plan-Neofluar 40×/1.30 Oil DIC and a Plan-Apochromat 63×/1.40 Oil DIC objective were utilized for cellular imaging and subcellular imaging, respectively.

2.8. Labeling cells with Pdots for flow cytometry.

Jurkat cells were labeled with streptavidin-functionalized PFP/PFPV Pdots by incubating 10^6 Jurkat T cells dispersed in labeling buffer (1xPBS, 1% BSA, 2 mM EDTA) with biotinylated primary anti-CD3 antibody for 30 min then with Pdot-SA (20 μg/mL) for 30 min, with two washes with labeling buffer after each incubation. The labeled cells were fixed in 0.6 mL of 4% (v/v) paraformaldehyde solution. A control sample was prepared by omitting the biotinylated primary anti-CD3 antibody. Flow cytometry was performed with a BD FACS Canto II flow cytometer (BD Biosciences; San Jose, CA, USA). A 405-nm laser was used for excitation; emission was collected through a BV450 channel (450/50 nm). Data was analyzed using FlowJo software.

2.9. Labeling cells with Pdots for cell imaging.

MCF-7 cells were labeled with PFP/PFPV Pdot-SA conjugates by plating cells on a 22×22-mm glass coverslip and culturing the cells to 60–70% confluence. The cells were fixed with 4% paraformaldehyde for 15 min and were blocked with BlockAid buffer for 30 min. The cells were then incubated with biotinylated primary anti-EpCAM antibody followed by 5 μg/mL Pdot-SA for 40 min each, with two washing steps after each incubation. A control sample was prepared by omitting the biotinylated primary anti-EpCAM antibody. Pdot-labeled cells were counterstained with the nuclear stain NucRed Live 647, fixed in 0.6 mL of 4% paraformaldehyde, washed, and imaged with a Zeiss LSM 510 fluorescence confocal microscope.

3. RESULTS AND DISCUSSION

We initially created non-FRET PFO, PFP, and PFPV Pdots by blending each of these commercially available polymers with PMSA. These Pdots had an average diameter of 20–30 nm based on DLS and TEM. As free polymers in THF solution, PFO, PFP, and PFPV

displayed high Φ values of 98%, 100%, and 94%, respectively. When the polymers were incorporated into Pdots, the absorption maxima ($\lambda_{abs,\ max}$) blue-shifted due to polymer coil formation and reduced effective conjugation length in Pdots relative to in solution (Figure S1).[28] The PFO, PFP, and PFPV Pdots exhibited low Φ values of 13.4%, 16.9%, and 6.0%. The photophysical properties of these Pdots are summarized in Table 1.

When PFPV was blended with PFO or PFP to form D/A Pdots (PFO/PFPV and PFP/PFPV; Figure 1), the maximum quantum yield increased dramatically, from 13.4% for PFO-only Pdots to 43.0% for PFO/PFPV Pdots, and from 16.9% for PFP-only Pdots to 73.1% for PFP/PFPV Pdots. In both cases, Φ was highest at the lowest acceptor concentration tested (2.5 mol% of total fluorophores: A/[D+A]×100%), and decreased with increasing acceptor polymer concentration (Figure 2). These FRET Pdots exhibited mainly acceptor emission, indicating efficient FRET. The PFP/PFPV Pdots retained a high σ due to a high donor polymer concentration of 97.5 mol%.

The maximum Φ for PFP/PFPV Pdots (73.1%) was higher than for PFO/PFPV Pdots (43.0%) due to greater spectral overlap of donor emission and acceptor absorbance for PFP/PFPV (Figure 2c–d). Coverage of donor emission by acceptor absorbance is a commonly used criterion for selecting D-A pairs; the coverage of acceptor absorbance by donor emission is sometimes overlooked but is also important for optimizing FRET efficiency. PFP emission provided greater coverage of PFPV acceptor absorption than did PFO emission (46% versus 23%). The PFP/PFPV pair also showed slightly greater coverage of donor emission by acceptor absorbance (89% versus 78%). The greater FRET efficiency in the PFP/PFPV Pdots was observed as a more rapid decrease in donor emission at 420 nm with increased PFPV concentration in PFP/PFPV Pdots than in PFO/PFPV Pdots (Figure 2e–f).

The difference in Pdot FRET efficiency can be understood in terms of the optical energy gap (E_g) for each polymer—the energy difference between ground state (S_0) energy and excited state (S_1) energy ($E_g=E_{S0\rightarrow S1}$),[29] which corresponds to the onset of the absorption spectrum of the polymer in the aggregation state.[30] The onset of absorption occurred at 435, 424, and 488 nm for the PFO, PFP, and PFPV Pdots, respectively, and the corresponding optical energy gaps were 2.85, 2.94, and 2.56 eV for PFO, PFP, and PFPV, calculated using the equation $E_{g,opt} = 1240/\lambda_{onset}$.[31] Jablonski diagrams (Figure 3) illustrate the mechanism of FRET in terms of electronic states and optical energy gaps.[32–35] Electrons in PFP and PFO are excited from ground state to excited state after irradiation near the $\lambda_{abs,\ max}$, and rapidly transfer energy to the more stable lower S_1 orbital through vibrational relaxation. In the presence of a suitable PFPV orbital, the donor fluorophore can non-radiatively transfer excited state energy to the acceptor through long-range dipole-dipole coupling.[36] The non-overlapping regions between the absorption of PFPV and emission of PFO and PFP are mainly in the ultraviolet range of the PFPV absorption band (Figure 2c–d); therefore, many of the high-energy PFPV chromophores cannot be excited by resonance energy transferred from the donor polymers.[28] PFP emission provides greater coverage of the PFPV absorption band (46%) than PFO emission (23%). Therefore, when the amount of PFPV is low (2.5 mol%), PFPV cannot absorb all of the energy from the PFO polymer chains through FRET. However, energy can be efficiently absorbed by PFPV from PFP as donor polymer because PFP has higher average excited states. Some energy transferred to PFPV can be transferred

back to the donor if the $E_{S0\rightarrow S1}$ of donor and acceptor are similar, which can lead to low FRET efficiency and energy loss due to competing aggregation-induced self-quenching of donors.

As free polymers in THF solution, PFO, PFP, and PFPV have extremely high Φ values (94–100%), indicating that light absorbed by the polymers is emitted as fluorescence with little energy loss. However, in Pdots, self-quenching due to chain entanglement is unavoidable. The overall Pdot quantum yield, Φ, is equal to Φ_{ET} (Energy transfer efficiency) × $\Phi_{acceptor}$. Values of $\Phi_{acceptor}$ for PFO/PFPV and PFP/PFPV Pdots with 2.5 mol% PFPV were both 90% when excited at the PFPV absorption side peak at 460 nm, indicating minimal self-quenching of PFPV. The $\Phi_{acceptor}$ values in PFO/PFPV and PFP/PFPV Pdots decreased significantly with increasing PFPV concentration. Pdot σ values at $\lambda_{abs,max}$ were similar and $\Phi_{acceptor}$ values were the same, but the overall Φ was greater for the PFP/PFPV Pdots than for the PFO/PFPV Pdots (Table 2), indicating greater Φ_{ET}. These results demonstrate the importance of selecting donor-acceptor pairs with large spectral overlap—including large coverage of both donor emission and acceptor absorbance—to obtain ultra-bright Pdots. The photophysical properties of these FRET-based Pdots are shown in Table 2.

To investigate the importance of reducing aggregation-induced self-quenching in optimizing Φ, a polymer without absorption at the PFO $\lambda_{abs,\ max}$ of 383 nm, poly[(2,3-dimethyl-1,4-phenylene)-co-(1,4-phenylene)] (PF; structure in Scheme S1), was blended with PFO at different concentrations during Pdot synthesis. When 30 mol% PF was added, Φ increased from 13.4% to 71.2% despite the reduced concentration of PFO (Table 2, Figure S2).

To improve the Φ and brightness of the PFO/PFPV Pdots, PFPV was replaced with a different acceptor polymer, PFBT, with greater spectral overlap with PFO. Replacing PFPV with PFBT yielded an increase in the maximum Φ from 43.0% for PFO/PFPV Pdots to 76.0% for PFO/PFBT Pdots; this maximum Φ value was obtained at 7.5 mol% PFBT (A/[D+A]) (Figure S3).

To create ultra-bright red-emitting Pdots, we added a second acceptor polymer, PFTBT, to enable cascade FRET in a PFO/PFBT/PBTBT ($D/A_1/A_2$) Pdot. This cascade FRET system yielded a maximum Φ of 64.2% at 5.0% PFTBT ($A_2/[D+A_1+A_2]$) and an overall PFO:BT:TBT molar ratio of 61:5:1, with an σ_R of 91.0%. The wide absorption band and lower optical band gap of the BT unit allowed it to effectively absorb energy from PFO via FRET (Table 2, Figure S3), and the TBT absorption and BT emission also overlap well, leading to efficient cascade FRET and ultra-bright red emission (Figure S4). Figure 4a summarizes the optical properties (σ_R, Φ, and B_R) of these and other Pdots synthesized in this study.

To explore the application of these ultra-bright Pdots as fluorescence probes for bioanalysis and bioimaging, we conjugated the PFP/PFPV Pdot with streptavidin, and labeled Jurkat T cells with the Pdots using biotinylated anti-CD3 antibodies. We used flow cytometry to verify the labeling and to check for nonspecific binding (Figure 4b). The results show that the streptavidin-functionalized Pdots effectively labeled CD3 receptors on Jurkat T cells with no nonspecific labeling observed in a control sample lacking the antibody. To test

the PFP/PFPV Pdot in a bioimaging application, MCF-7 breast-cancer cells were labeled with streptavidin-functionalized Pdots and with biotinylated anti-EpCAM antibodies, and were imaged using confocal fluorescence microscopy (Figure 5). The results showed that the Pdots effectively labeled EpCAM receptors on the MCF-7 cell surface. In a control in which the biotinylated primary antibody was absent, no fluorescence was detected (Figure 5a), confirming the specificity of the labeling.

4. CONCLUSIONS

We achieved ultra-bright FRET-based Pdots by use a small, optimized amount of acceptor polymer in D/A and D/A_1/A_2 (cascade FRET) Pdots, and by selecting donor-acceptor pairs with large coverage of both donor emission and acceptor absorbance. This approach can be generalized to create ultra-bright Pdots with emissions that span the visible spectrum for use in bioanalysis and bioimaging applications.

Supplementary Material

Refer to Web version on PubMed Central for supplementary material.

ACKNOWLEDGMENTS

We gratefully acknowledge support of this work by the National Institutes of Health (R01MH115767 and R01MH113333) and the University of Washington.

REFERENCES

(1). Wu C; Hansen SJ; Hou Q; Yu J; Zeigler M; Jin Y; Burnham DR; McNeill JD; Olson JM; Chiu DT Design of Highly Emissive Polymer Dot Bioconjugates for In Vivo Tumor Targeting. Angew. Chem 2011, 123 (15), 3492–3496.

(2). Yu J; Rong Y; Kuo C-T; Zhou X-H; Chiu DT Recent Advances in the Development of Highly Luminescent Semiconducting Polymer Dots and Nanoparticles for Biological Imaging and Medicine. Anal. Chem 2017, 89 (1), 42–56. [PubMed: 28105818]

(3). Chen L; Chen D; Jiang Y; Zhang J; Yu J; DuFort CC; Hingorani SR; Zhang X; Wu C; Chiu DT A BODIPY-Based Donor/Donor–Acceptor System: Towards Highly Efficient Long-Wavelength-Excitable Near-IR Polymer Dots with Narrow and Strong Absorption Features. Angew. Chem. Int. Ed 2019, 58 (21), 7008–7012.

(4). Wu C; Chiu DT Highly Fluorescent Semiconducting Polymer Dots for Biology and Medicine. Angew. Chem. Int. Ed 2013, 52 (11), 3086–3109.

(5). Chen H; Yu J; Zhang J; Sun K; Ding Z; Jiang Y; Hu Q; Wu C; Chiu DT Monitoring Metabolites Using an NAD(P)H-sensitive Polymer Dot and a Metabolite-specific Enzyme. Angew. Chem 2021, ange.202106156.

(6). Feng G; Fang Y; Liu J; Geng J; Ding D; Liu B Multifunctional Conjugated Polymer Nanoparticles for Image-guided Photodynamic and Photothermal Therapy. Small 2017, 13 (3), 1602807.

(7). Li J; Rao J; Pu K Recent Progress on Semiconducting Polymer Nanoparticles for Molecular Imaging and Cancer Phototherapy. Biomaterials 2018, 155, 217–235. [PubMed: 29190479]

(8). Li J; Pu K Development of Organic Semiconducting Materials for Deep-Tissue Optical Imaging, Phototherapy and Photoactivation. Chem. Soc. Rev 2019, 48 (1), 38–71. [PubMed: 30387803]

(9). Wang J; Lv F; Liu L; Ma Y; Wang S Strategies to Design Conjugated Polymer Based Materials for Biological Sensing and Imaging. Coord. Chem. Rev 2018, 354, 135–154.

(10). Senthilkumar T; Zhou L; Gu Q; Liu L; Lv F; Wang S Conjugated Polymer Nanoparticles with Appended Photo-Responsive Units for Controlled Drug Delivery, Release, and Imaging. Angew. Chem. Int. Ed 2018, 57 (40), 13114–13119.

(11). Jiang Y; Pu K Multimodal Biophotonics of Semiconducting Polymer Nanoparticles. Acc. Chem. Res 2018, 51 (8), 1840–1849. [PubMed: 30074381]

(12). Wu C; Schneider T; Zeigler M; Yu J; Schiro PG; Burnham DR; McNeill JD; Chiu DT Bioconjugation of Ultrabright Semiconducting Polymer Dots for Specific Cellular Targeting. J. Am. Chem. Soc 2010, 132 (43), 15410–15417. [PubMed: 20929226]

(13). Hong G; Antaris AL; Dai H Near-Infrared Fluorophores for Biomedical Imaging. Nat. Biomed. Eng 2017, 1 (1), 0010.

(14). Pu K; Shuhendler AJ; Jokerst JV; Mei J; Gambhir SS; Bao Z; Rao J Semiconducting Polymer Nanoparticles as Photoacoustic Molecular Imaging Probes in Living Mice. Nat. Nanotechnol 2014, 9 (3), 233–239. [PubMed: 24463363]

(15). Jiang Y; Hu Q; Chen H; Zhang J; Chiu DT; McNeill J Dual-Mode Superresolution Imaging Using Charge Transfer Dynamics in Semiconducting Polymer Dots. Angew. Chem. Int. Ed 2020, 59 (37), 16173–16180.

(16). Sun Z; Liu Z; Chen H; Li R; Sun Y; Chen D; Xu G; Liu L; Wu C Semiconducting Polymer Dots with Modulated Photoblinking for High-Order Super-Resolution Optical Fluctuation Imaging. Adv. Optical Mater 2019, 7, 1900007.

(17). Hide F; Díaz-García MA; Schwartz BJ; Heeger AJ New Developments in the Photonic Applications of Conjugated Polymers. Acc. Chem. Res 1997, 30 (10), 430–436.

(18). Pu K-Y; Li K; Liu B A Molecular Brush Approach to Enhance Quantum Yield and Suppress Nonspecific Interactions of Conjugated Polyelectrolyte for Targeted Far-red/Near-infrared Fluorescence Cell Imaging. Adv. Funct. Mater 2010, 20 (17), 2770–2777.

(19). Piwonski H; Li W; Wang Y; Michinobu T; Habuchi S Improved Fluorescence and Brightness of Near-Infrared and Shortwave Infrared Emitting Polymer Dots for Bioimaging Applications. ACS Appl. Polym. Mater 2019, 2 (2), 569–577.

(20). Verma M; Chan Y-H; Saha S; Liu M-H Recent Developments in Semiconducting Polymer Dots for Analytical Detection and NIR-II Fluorescence Imaging. ACS Appl. Bio Mater 2020, 4 (3), 2142–2159.

(21). Zhang X; Yu J; Rong Y; Ye F; Chiu DT; Uvdal K High-Intensity Near-IR Fluorescence in Semiconducting Polymer Dots Achieved by Cascade FRET Strategy. Chem. Sci 2013, 4 (5), 2143. [PubMed: 28959389]

(22). Rong Y; Wu C; Yu J; Zhang X; Ye F; Zeigler M; Gallina ME; Wu I-C; Zhang Y; Chan Y-H; Sun W; Uvdal K; Chiu DT Multicolor Fluorescent Semiconducting Polymer Dots with Narrow Emissions and High Brightness. ACS Nano 2013, 7 (1), 376–384. [PubMed: 23282278]

(23). Chen C-P; Huang Y-C; Liou S-Y; Wu P-J; Kuo S-Y; Chan Y-H Near-Infrared Fluorescent Semiconducting Polymer Dots with High Brightness and Pronounced Effect of Positioning Alkyl Chains on the Comonomers. ACS Appl. Mater. Interfaces 2014, 6 (23), 21585–21595. [PubMed: 25394668]

(24). Jares-Erijman EA; Jovin TM FRET Imaging. Nat. Biotechnol 2003, 21 (11), 1387–1395. [PubMed: 14595367]

(25). Ravets S; Labuhn H; Barredo D; Béguin L; Lahaye T; Browaeys A Coherent Dipole–Dipole Coupling between Two Single Rydberg Atoms at an Electrically-Tuned Förster Resonance. Nat. Phys 2014, 10 (12), 914–917.

(26). Förster T Zwischenmolekulare Energiewanderung Und Fluoreszenz. Ann. Phys 1948, 437 (1–2), 55–75.

(27). Ye F; White CC; Jin Y; Hu X; Hayden S; Zhang X; Gao X; Kavanagh TJ; Chiu DT Toxicity and oxidative stress induced by semiconducting polymer dots in RAW264. 7 mouse macrophages. Nanoscale 2015, 7 (22), 10085–10093. [PubMed: 25978523]

(28). Sun K; Chen H; Wang L; Yin S; Wang H; Xu G; Chen D; Zhang X; Wu C; Qin W Size-Dependent Property and Cell Labeling of Semiconducting Polymer Dots. ACS Appl. Mater. Interfaces 2014, 6 (13), 10802–10812. [PubMed: 24930393]

(29). Costa JCS; Taveira RJS; Lima CFRAC; Mendes A; Santos LMNBF Optical Band Gaps of Organic Semiconductor Materials. Opt. Mater 2016, 58, 51–60.

(30). Chen X; Marks A; Paulsen BD; Wu R; Rashid RB; Chen H; Alsufyani M; Rivnay J; McCulloch I N-Type Rigid Semiconducting Polymers Bearing Oligo (Ethylene Glycol) Side Chains for High-Performance Organic Electrochemical Transistors. Angew. Chem. Int. Ed 2021, 60 (17), 9368–9373.

(31). Dittmer A; Izsák R; Neese F; Maganas D Accurate Band Gap Predictions of Semiconductors in the Framework of the Similarity Transformed Equation of Motion Coupled Cluster Theory. Inorg. Chem 2019, 58 (14), 9303–9315. [PubMed: 31240911]

(32). Rajdev P; Ghosh S Fluorescence Resonance Energy Transfer (FRET): A Powerful Tool for Probing Amphiphilic Polymer Aggregates and Supramolecular Polymers. J. Phys. Chem. B 2018, 123 (2), 327–342. [PubMed: 30407823]

(33). Shrestha D; Jenei A; Nagy P; Vereb G; Szöllősi J Understanding FRET as a Research Tool for Cellular Studies. Int. J. Mol. Sci 2015, 16 (4), 6718–6756. [PubMed: 25815593]

(34). Chen C; Ou H; Liu R; Ding D Regulating the Photophysical Property of Organic/Polymer Optical Agents for Promoted Cancer Phototheranostics. Adv. Mater 2020, 32 (3), 1806331.

(35). Hochreiter B; Kunze M; Moser B; Schmid JA Advanced FRET Normalization Allows Quantitative Analysis of Protein Interactions Including Stoichiometries and Relative Affinities in Living Cells. Sci. Rep 2019, 9 (1), 1–16. [PubMed: 30626917]

(36). Liu B; Bazan GC Optimization of the Molecular Orbital Energies of Conjugated Polymers for Optical Amplification of Fluorescent Sensors. J. Am. Chem. Soc 2006, 128 (4), 1188–1196. [PubMed: 16433535]

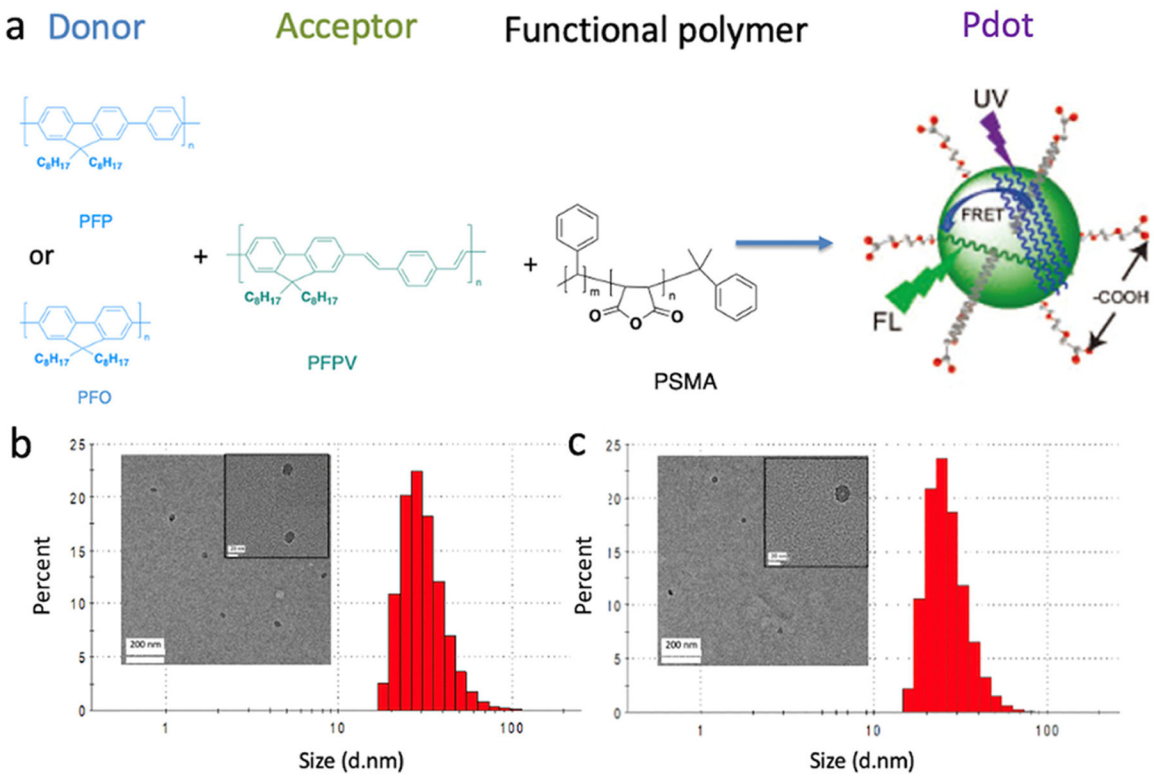

Figure 1.

(a) Synthesis of FRET-based Pdots. Donor (PFP or PFO) and acceptor (PFPV) polymers were blended with the surfactant polymer PSMA, yielding surface carboxyl groups for cell conjugation. (b-c) Size distributions of (b) PFO/PFP Pdots (2.5 mol% PFP) and (c) PFP/PFPV Pdots (2.5 mol% PFPV) based on DLS (inset: TEM images).

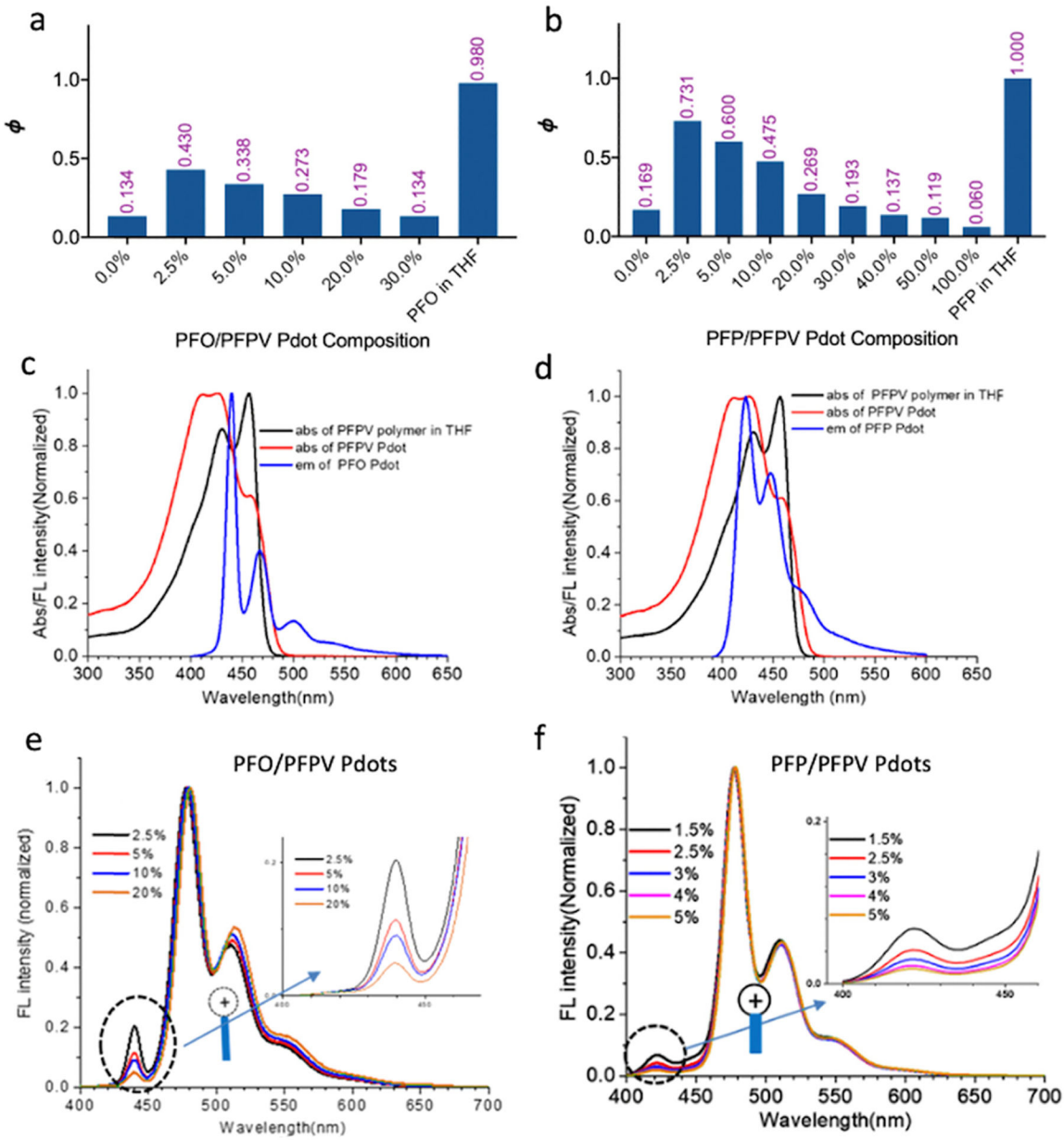

Figure 2.

Ultra-bright green-emitting Pdots. (a) Quantum yield of PFO/PFPV Pdots as a function of PFPV concentration. Free PFO in THF is shown at the far right. (b) Quantum yield of PFP/PFPV Pdots as a function of PFPV concentration. Free PFP in THF is shown at the far right. (c) Overlap of PFO Pdot emission with PFPV Pdot absorption. The absorption spectrum of PFPV in THF is also shown. (d) Overlap of PFP Pdot emission with PFPV Pdot absorption. (e) Emission spectra of PFO/PFPV Pdots containing 2.5–20 mol% PFPV. (f) Emission spectra of PFP/PFPV Pdots containing 1.5–5.0 mol% PFPV.

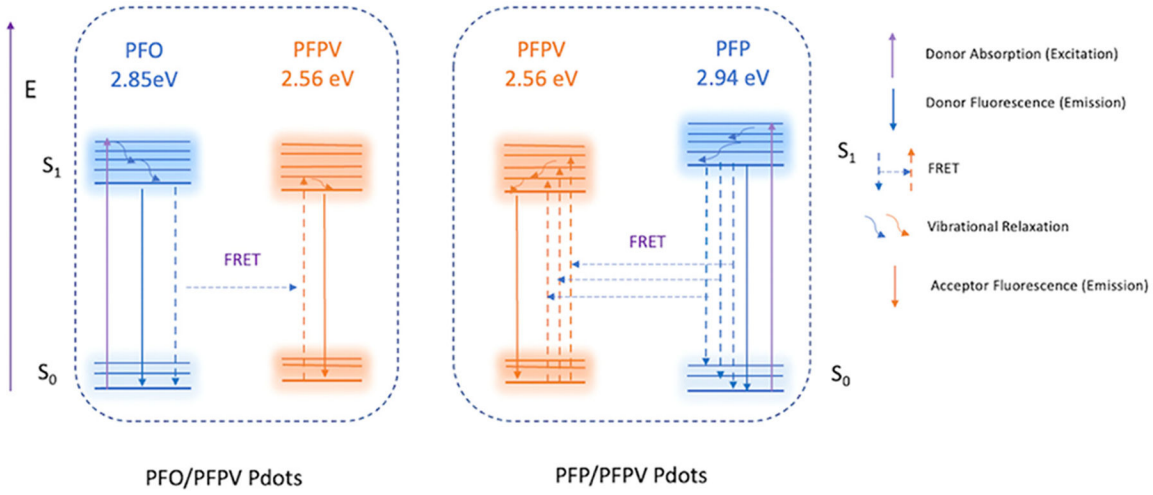

Figure 3.

Jablonski diagram illustrating the mechanism of FRET in PFO/PFPV and PFP/PFPV Pdots. Greater FRET efficiency was observed in the PFP/PFPV Pdots than in the PFO/PFPV Pdots.

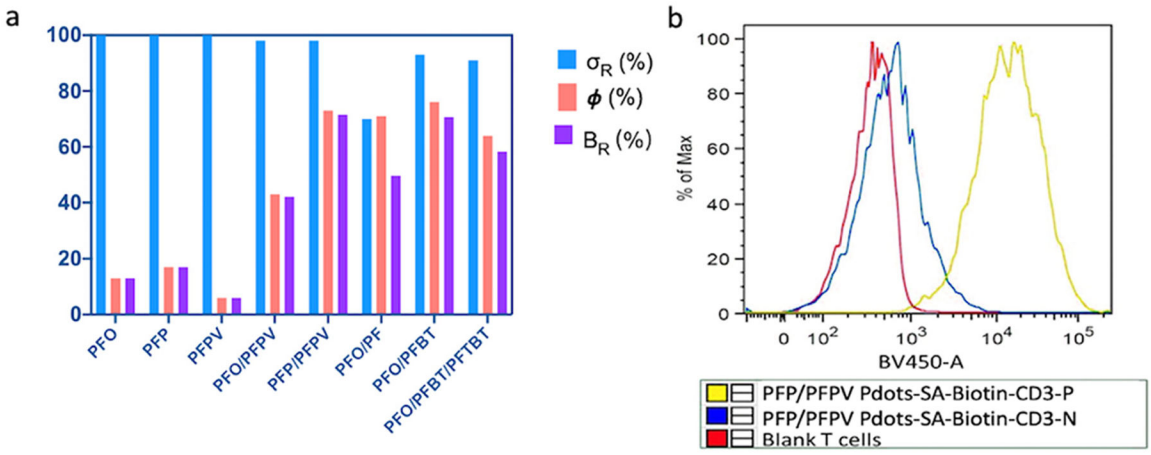

Figure 4.

(a) Relative absorbance cross section (σ_R), quantum yield (Φ), and relative brightness (B_R) of various Pdots. (b) Flow cytometry analysis of T cells conjugated with streptavidin-PFP/PFPV Pdots via a biotinylated anti-CD3 antibody (yellow), a negative control lacking the antibody (blue), and blank (unlabeled) T cells (red).

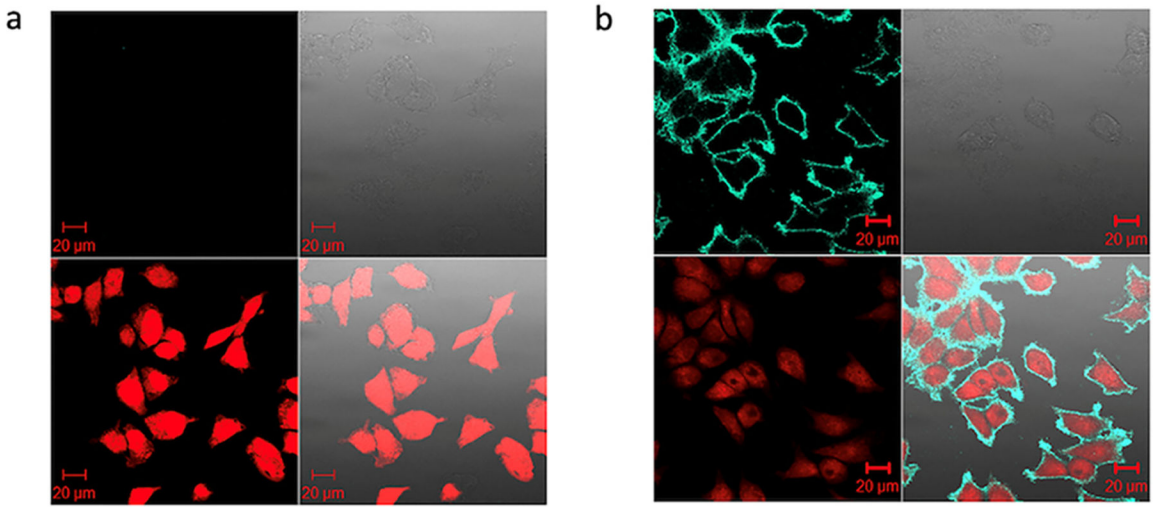

Figure 5.

Confocal fluorescence microscopy of MCF-7 breast-cancer cells labeled with streptavidin-functionalized PFP/PFPV Pdots and biotinylated anti-EpCam antibody. (a) Negative control lacking the biotinylated primary antibody. (b) Labeling with both PFP/PFPV Pdot-streptavidin and biotinylated primary antibody. In both sets of four images: upper left: green channel; upper right: differential interference contrast images; lower left: nuclear stain with NucRed Live 647; lower right: combined fluorescence images. Scale bars, 20 μm.

Table 1.

Photophysical properties of non-FRET Pdots.

Pdot	$\lambda_{abs,\,max}$ [nm]	$\lambda_{PL,\,max}$ [nm]	λ_{onset} [nm]	$E_{g,opt}$ [a] [eV]	Φ [%]	Size [b] [nm]	ζ potential [meV]
PFO	383	438	451	2.75	13.4	26	−30.2
PFP	373	422	424	2.92	16.9	24	−34.5
PFPV	427	478	488	2.54	6.0	29	−29.8

[a] $E_{g,opt}$ (optical energy gap) = $1240/\lambda_{onset}$.

[b] Average hydrodynamic diameter based on DLS.

Table 2.

Photophysical properties of FRET-based Pdots.

Pdot (D/A or D/A_1/A_2)	**$\lambda_{abs\ max}$ [nm]**	**$\lambda_{PL\ max}$ [nm]**	**Stokes shift [nm]**	**σ_R [%]** *a*	**Φ [%]**	**Size [nm]**	**B_R [%]** *b*
PFO/PFPV-2.5 mol% *c*	383	478	95	97.5	43.0	26	41.9
PFP/PFPV-2.5 mol%	373	478	105	97.5	73.1	29	71.7
PFO/PF-30.0 mol%	383	440	57	70.0	71.2	28	49.7
PFO/PFBT-BT-7.5 mol%	383	547	164	92.5	76.0	19	70.3
PFO/PFBT/PFTBT-TBT-1.5 mol%	384	630	246	91.0	64.2	23	58.2

a σ_R (relative absorbance cross section) = $\sigma_{abs}/\sigma_{all}$.

b B_R (relative brightness) = $\sigma_R \times \Phi$.

c Mol% values for acceptor polymer (A or A_2).